

Article

Meteorological-Data-Based Modeling for PV Performance Optimization

Mahmood Alharbi ^{1,*} , Ramzi Alahmadi ² and Ahmed Alahmadi ¹¹ Electrical Engineering Department, Taibah University, Medinan 42353, Saudi Arabia² Industrial Engineering Department, Taibah University, Medinan 42353, Saudi Arabia

* Correspondence: mamharbi@taibahu.edu.sa

Abstract: Developing a sustainable and reliable photovoltaic (PV) energy system requires a comprehensive analysis of solar profiles and an accurate prediction of solar energy performance at the study site. Installing the PV modules with optimal tilt and azimuth angles has a significant impact on the total irradiance delivered to the PV modules. This paper proposes a comprehensive optimization model to integrate total irradiance models with the PV temperature model to find the optimal year-round installation parameters of PV modules. A novel integration between installation parameters and the annual average solar energy is presented, to produce the maximum energy output. The results suggest an increase in energy yields of 4% compared to the conventional scheme, where tilt angle is equal to the latitude and the PV modules are facing south. This paper uses a real-time dataset for the NEOM region in Saudi Arabia to validate the superiority of the proposed model compared to the conventional scheme, but it can be implemented as a scheme wherever real-time data are available.

Keywords: energy conversion; power generation meteorological factors; photovoltaic cell radiation effects; photovoltaic cell thermal factors; optimization methods; modeling; algorithms



check for updates

Citation: Alharbi, M.; Alahmadi, R.; Alahmadi, A. Meteorological-Data-Based Modeling for PV Performance Optimization. *Sustainability* **2023**, *15*, 8659. <https://doi.org/10.3390/su15118659>

Academic Editors: Francesco Calise, Maria Vicidomini, Rafał Figaj and Francesco Liberato Cappiello

Received: 12 January 2023

Revised: 31 March 2023

Accepted: 28 April 2023

Published: 26 May 2023



Copyright: © 2023 by the authors. Licensee MDPI, Basel, Switzerland. This article is an open access article distributed under the terms and conditions of the Creative Commons Attribution (CC BY) license (<https://creativecommons.org/licenses/by/4.0/>).

1. Introduction

In addition to energy challenges related to the depletion of fossil fuels and their implications for energy security and sustainability, new challenges have emerged. For example, the impact of greenhouse gas emissions from fossil fuels on the global climate system is a rising concern to the international community. In addition, the high air pollution caused by the intensive use of fossil fuels, and its implications for public health, is alarming to many countries. A major transition to low-carbon energy systems is essential to mitigate the greenhouse gases caused by fossil fuels [1]. Therefore, there serious interest exists in regard to reducing the impact of fossil fuel emissions. In 2015, 190 countries signed the Paris Agreement, which is a commitment to reduce emissions of carbon dioxide (CO₂), the underlying cause of greenhouse gases (GHG) [2], from fossil fuels. The agreement set an ambitious target to reach net-zero carbon emissions by 2050.

The intensive use of fossil fuels for energy has been challenging to the energy sector [3]. The growth in annual energy demand was estimated to increase by 1.3% each year until 2040 [4]. However, the global energy demand recorded a 5.4% increase in 2021 alone, as the world economy recovered from COVID-19 at an unprecedented rate, while energy intensity improvements stalled during the pandemic. The surging demand for energy in 2021 was mostly met by fossil fuels, which resulted in a record high of annual-basis increase in global CO₂ emissions, adding more challenges to the progress toward the global objective of net-zero carbon emission by 2050 [5,6].

The energy and energy-related challenges have to be comprehensively addressed through studies that identify strategies and solutions that may help to achieve sustainable and efficient systems that have lower carbon emissions [7]. In this context, increasing the share of renewable energies in the energy mix is crucial for a sustainable supply

for the energy demand, while maintaining the mission of curbing greenhouse gases [8]. Installation of renewable energy systems is continuously achieving annual record growth, despite unforeseen disruptions. In 2021, for instance, a record annual increase of 17% in the renewables capacity was achieved. The total installed capacity reached 3146 GW, which was mainly driven by solar photovoltaic (PV) and wind power, despite the increased delivery lead time, increased prices of solar and wind energy system components, and the unprecedented supply chain disruption caused by COVID-19. In 2021, 28.5% of the world's electricity demand was supplied by renewable energies, yet, with the surging energy demand, most of the demand was met by fossil fuels, accounting for around 80%. Only 20% of the demand was met by renewables, mainly solar and wind energy sources, which is far from the required progress to achieve the mission of net-zero carbon emission by 2050 [6].

Many studies suggest the domination of solar and wind energy in regard to total renewable energy potential [9], however, the evaluation of the available renewable energy sources that can be sustainably harvested is decisive [7]. Different constraints exist that affect the extractable net renewable energy, including intermittency [9] and land occupation constraints [10]. With regards to the economics, ref. [11] emphasize the importance of considering the renewable energy availability constraints prior to assessing the energy return on investment (EROI) in renewable energy. In their work, they used a global grid-cell approach to assess the global net solar energy potential. Of the constrained available global solar energy, which is significantly lower than previous estimates, EROI ratios of only 5, 7.5, and 9 can be achieved if 98%, 75%, and 15% of the available solar energy is extracted, respectively.

The high constraints impacting renewable energy availability, the technical efficiency, and the economic barriers [12], create a need for an optimized utilization of renewable energy systems. In the case of solar energy, which is the focus of this paper, numerous technology and scenario configurations exist that impact the parameters leading to the achievement of different harvesting levels of solar energy potential. In this context, different cell technologies are estimated to deliver distinct cell efficiencies. In a survey of solar cell supply companies for 2020, p-type monocrystalline silicon (p-type mono-si) cells were estimated to deliver 22.8% efficiency, while multicrystalline silicon (mc-si) cells had a lower average efficiency, estimated at 20.8% [13].

In addition, installation of fixed-tilt solar PV systems versus those installed with tracking capability is estimated to deliver different solar module efficiencies [14]. Solar systems with tracking capabilities outperform fixed-tilt systems due to their ability to follow the sun's movement and, thus, maximize the solar irradiation reaching the surface of the solar panels. However, the tracking systems are rarely cost effective due to their high cost and demand for energy for operation. Therefore, cyclic adjustments of the solar panels elevations to the optimal tilt angles related to the horizon is an applicable way to optimize the output of the solar systems [15].

The problem of finding the optimal tilt angle has been a research interest for decades. Over the years, the problem of specifying the optimal tilt angle has been investigated through different approaches for different locations. Some researchers have treated the optimal tilt as a function of latitude only [16–18], while [19] formulated the optimal tilt angle as a function of latitude, type of energy demand, and weather characteristics. Qualitative, analytical, and quantitative treatments for the problem are continually being explored in the literature [20–25].

When it comes to specifying the optimal tilt angle for the best solar irradiance collection, a wide range of optimal tilt angles have been recommended in the literature, mostly for specific locations, months, and seasons. Ref. [26] recommended, for Lhasa, China, an optimal tilt angle fixed at 50°. Ref. [15] concluded that, for Madinah, Saudi Arabia, the optimal tilt angles for spring, summer, fall, and winter were 17°, 12°, 28°, and 37°, respectively. Similarly, ref. [27] recommended that the optimal tilt angles for winter and summer were 43.3° and nearly flat, respectively, which is about the latitude $\pm 15^\circ$.

Likewise, the optimal fixed tilt angle for solar panels has been widely recommended in relation to the latitude of the location. Ref. [15] concluded that the optimal annual average tilt angle for Madinah, Saudi Arabia, is 23.5° , which is relatively close to Madinah's latitude of 24.5° . Ref. [28] suggested that the optimal fixed tilt angle in Jeddah, Saudi Arabia, should be 24.5° , which corresponds to the latitude of Jeddah (21.5°). Similar results were found for different locations, such as Ontario, Canada [29], New Delhi, India [30], Kuala Lumpur, Malaysia [31], and different cities in Saudi Arabia [32].

Despite the wide consensus in the literature on the relativity between the annual optimal tilt angle and the conventional orientation (latitude), it has been suggested that fixing the solar collector at an angle equal to the location's latitude could considerably limit the full utilization of the solar collection system. A study conducted by [33], for 18 locations in Saudi Arabia, concluded that the optimal tilt angle was significantly different from the latitude. Ref. [34] concluded that for San Francisco and Paris, a potential increase of 2.04% and 7.38%, respectively, could be achieved in yielded energy by optimizing the tilt angle compared to a fixed tilt angle corresponding to the latitude. Ref. [30] estimated that using a yearly average fixed tilt angle (latitude) resulted in a 15% loss in achievable energy compared to a monthly adjustment of the tilt angle.

Similarly, different conclusions have been reached regarding the effectiveness of monthly adjustments of the optimal tilt angle on the gains in collected solar energy. The results derived by [35] demonstrate that different monthly adjustments of the optimal tilt angle delivered significant changes in solar energy gains. They concluded that, for Dhaka, Bangladesh, a 15% average annual increase existed in the output of the solar energy system through monthly adjustments of the optimal tilt angle. Similarly, ref. [33] conducted a study on 18 different locations in Saudi Arabia and concluded that, for Riyadh, a 4.01% energy yield could be achieved through monthly adjustments of the optimal tilt angles.

On the other hand, ref. [26] reported a diminished significance of monthly adjustments of the optimal tilt angle on solar energy gains in their study carried out during the heating season (i.e., November 15 to March 15) in Lhasa, China. While the monthly optimal tilt angles were 50° , 60° , 60° , 50° , and 30° for November, December, January, February, and March, respectively, the change in solar energy gains was not significant. The five monthly tilt angle adjustments, at a fixed azimuth angle of 5° , did not exceed a maximum increase of 1.1% in the collected hourly average solar irradiance. Likewise, ref. [36] conducted a study to analyze the optimal tilt angle for a fixed building integrated photovoltaic (BIPV) system, south oriented tilted roof, at 20 different locations in 14 countries, and found that more than 98.5% of the system's performance can be obtained using a tilt angle identical to the location's latitude. Mixed results are reported in the literature regarding the optimal tilt angle. In addition, the solar panel's surface orientation (azimuth angle) is commonly assumed to be facing towards the equator when finding the optimal tilt angle, or the optimal tilt and azimuth angles are separately determined.

By considering the effects of both ambient temperature and wind speed on the temperature of photovoltaic modules, this work introduces a novel multi-objective optimization methodology to explore the optimal tilt angle and optimum azimuth angles simultaneously. Then, the output of the solar irradiance model and the PV temperature model are used, in conjunction with an equivalent electric circuit model and maximum power point tracking (MPPT), to provide a comprehensive estimate of the induced power density and annual energy, based on real-time meteorological data. Any site where a PV system is planned to be installed is suitable for the proposed project. Here, a cluster of sites has been determined using the proposed methodology, and the results are compared to those obtained using the conventional approach.

The remainder of this paper is structured as follows. The state-of-the-art solar irradiance, PV temperature, and energy yield prediction models are reviewed in Section 2. In Section 3, the results of the models presented in Section 2 are discussed. Section 4 concludes this paper.

2. PV Performance Investigation Methodology

For optimizing the PV output power and energy, a modeled process is implemented using MATLAB. Figure 1 represents the flowchart for the optimization process. It starts with defining the input data for a certain location and the PV module specifications for the certain manufactured model intended to be applied. The input data consists of solar data (irradiance and angles) and meteorological data (ambient temperature and wind speed). The solar data, with the range set of optimization factors (tilt β and azimuth γ), are taken into the solar irradiance model (Section 2.1). Next, the output of the solar irradiance model with the absorbed total global horizontal irradiance GHI_t , with both meteorological data and selected PV module specifications, are inserted into the PV temperature model (Section 2.2), resulting in the absorbed cell temperature T_c . This, combined with previous results, becomes the input of the PV equivalent electric circuit model (Section 2.3), which results in different values of PV output, in which several iterations are run, based on the range values of both β and γ , to find their optimum values.

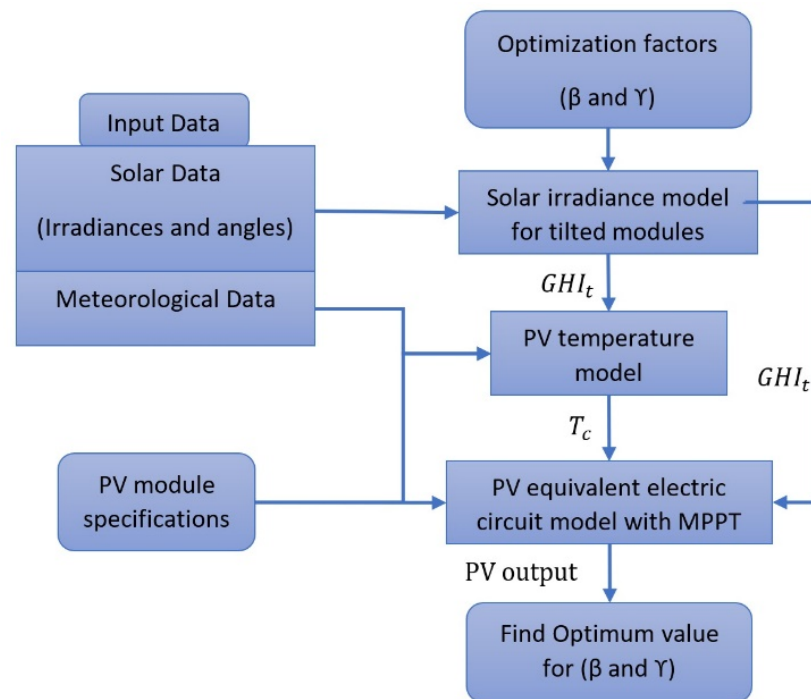


Figure 1. Modeling flowchart for PV performance optimization.

2.1. Solar Irradiance Model

The meteorological data collected by the King Abdullah City for Atomic and Renewable Energy (KACARE) consists of different types of solar intensity, which are global horizontal irradiance (GHI), direct normal irradiance (DNI), and diffuse horizontal irradiance (DHI). GHI is the sum of both DNI and DHI on a horizontal surface. However, in this model, having more estimation accuracy requires recalculating the global irradiance to be compatible with the tilted surface (i.e., the tilted PV panel). The solar irradiance model on the tilted surface can be represented by either an isotropic or an anisotropic sky model. In this research, an isotropic sky model was utilized, since the distribution of the diffuse irradiance from the sky is assumed to be received uniformly [37,38]. The following equation defined the total global irradiance on a tilted surface (GHI_t) as the sum of direct irradiance (DNI_t), diffuse irradiance (DHI_t), and reflected irradiance (RI_t).

$$GHI_t = DNI_t + DHI_t + RI_t. \quad (1)$$

The direct irradiance on the tilted surface, DNI_t , can be written as:

$$DNI_t = DNI \cdot R_b, \quad (2)$$

where R_b is the geometric factor that represents the beam radiation ratio of a tilted to a horizontal surface at any time [37]. This factor can be expressed as:

$$R_b = \frac{\cos \theta}{\sin \theta_z}, \quad (3)$$

where θ is the incidence angle of the directed normal radiation to a surface and, as in [4], $\cos \theta$ represents the relationship between the sun's position and a plane on the earth in terms of several angles, such as the zenith angle, θ_z , illustrated in Figure 2 [37].

$$\begin{aligned} \cos \theta = & \sin \delta \sin \phi \cos \beta - \sin \delta \sin \phi \sin \beta \cos \gamma \\ & + \cos \delta \cos \phi \cos \beta \cos \omega + \cos \delta \sin \phi \sin \beta \cos \gamma \cos \omega \\ & + \cos \delta \sin \phi \sin \beta \sin \omega, \end{aligned} \quad (4)$$

where all the angles are defined in Table 1 and Figure 2.

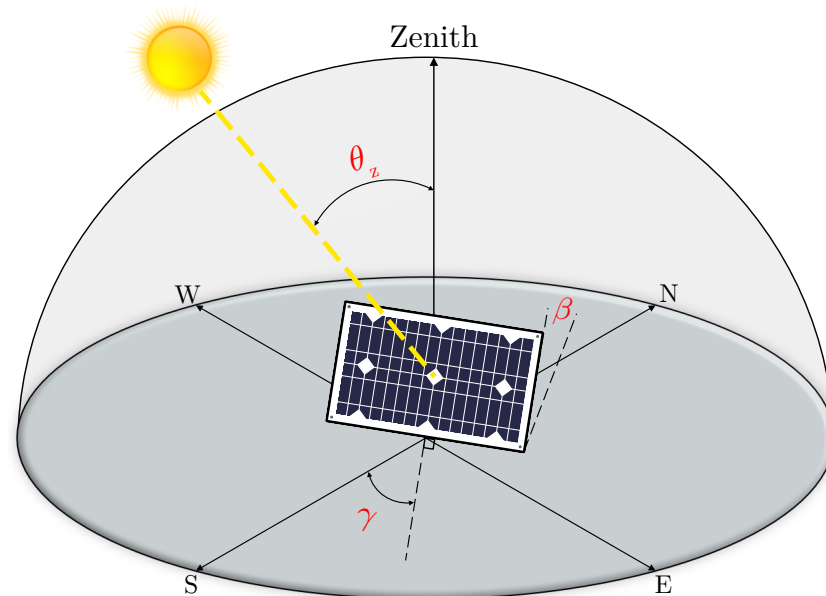


Figure 2. Zenith, azimuth, and PV module tilt angles.

The solar declination can be expressed as:

$$\delta = 23.45 \sin\left(360 \frac{284 + n}{365}\right), \quad (5)$$

where n is the day number during the year (i.e., 1 to 365).

The second term in (1) is the diffuse irradiance on a tilted PV module, DHI_t , which is expressed as:

$$DHI_t = DHI \cdot R_{df}, \quad (6)$$

where R_{df} is a geometric factor that represents the diffuse radiation ratio of a tilted to a horizontal surface at any time [37]. This factor can be expressed as:

$$R_{df} = \frac{1 + \cos \beta}{2}. \quad (7)$$

Table 1. Definitions of angles related to the angular position of the sun and PV panel.

Symbol	Definition	Value Range
δ	Declination (angle between the plane of the equator and straight line drawn from the sun [1]), expressed in (5)	-23.45° to 23.45°
ϕ	Latitude (south or north of the equator)	-90° to 90°
β	Tilt angle (between PV panel and the surface)	0° to 90°
γ	Azimuth angle of the panel (refer to south, -ve in east rotation and +ve in west rotation)	-180° to 180°
ω	Hour angle (before -ve or after +ve solar noon)	15° per hour
θ_z	Zenith angle (incidence angle of the beam radiation on the horizontal surface)	0° to 90°

The last term in (1) represents the reflected irradiance, RI_t , which depends on the nature of the Earth and surrounding circumstances. The measurement of these impacts are evaluated using the geometric factor, R_r , and the irradiance reflection coefficient (i.e., albedo factor), ρ [37].

$$RI_t = RI \cdot R_r \cdot \rho, \quad (8)$$

where

$$R_r = \frac{1 - \cos \beta}{2}. \quad (9)$$

2.2. PV Temperature Model

The temperature of the PV cell has a key impact on the PV performance. Three variables play a role in changing the PV cell temperature (T_c): solar radiation (G_T), ambient temperature (T_a), and wind speed (v_w) [37,39]. The following function defines the relationship between those factors and the cell temperature, which can be determined from:

$$\frac{T_c - T_a}{T_{NOCT} - T_{a,NOCT}} = \frac{G_T}{G_{NOCT}} \frac{9.5}{(5.7 + 3.8v_w)} \left[1 - \frac{\eta_c}{(\tau\alpha)}\right], \quad (10)$$

where:

- T_{NOCT} : the nominal operating cell temperature when the ambient temperature is 20°C , solar radiation is 0.8 kW/m^2 , and the local wind speed is 1 m/s ;
- $T_{a,NOCT}$: ambient temperature at the nominal operating condition (20°C);
- G_T : total global irradiance on a tilted PV module (GHI_t);
- G_{NOCT} : solar radiation at nominal operating condition (0.8 kW/m^2);
- v_w : local wind speed in meters per second;
- η_c : module efficiency under standard test conditions, STC; and
- $\tau\alpha$: effective coefficient of transmittance (τ)–absorptance (α) product of the cells.

2.3. PV Equivalent Electric Circuit Model and MPP Tracker

After determining both the irradiance that was delivered to the PV module and the PV cell temperature, as discussed in Sections 2.1 and 2.2, the electric power generated by the PV module needs to be estimated in order to determine the PV performance. Thus, in this section, an equivalent electric circuit for the PV cell and a maximum power point tracking algorithm are discussed.

By modeling the PV equivalent electric circuit, the output voltage and current can be determined. There are different electrical PV circuits for predicting PV cell output power, such as the single-diode (SD) PV model, double-diode (DD) PV model, and tri-diode (TD) PV model, as discussed in [40]. Here, we choose the single-diode equivalent circuit

model, shown in Figure 3, as a commonly used example in the literature [41]. However, the proposed method in this paper is general and can easily be applied to the other model types.

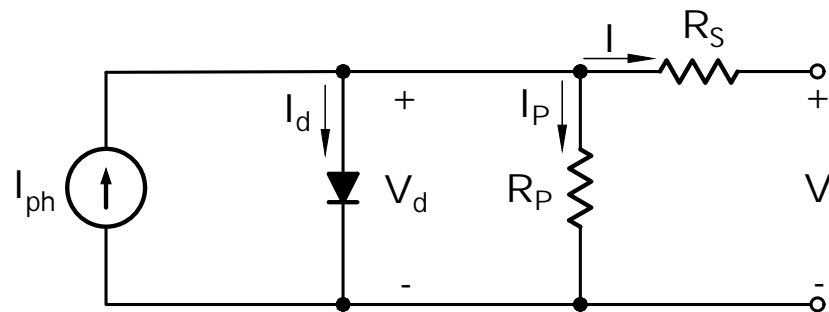


Figure 3. Equivalent circuit model for a PV cell.

As illustrated in Figure 3, the equivalent circuit includes the dependent current source due to the photon delivered to the cell from the sunlight (I_{ph}), the p–n junction diode resulting from the fabrication of the semiconductor, and internal series and parallel resistances (R_S , R_P).

The output current (I) of each cell is described by:

$$\begin{aligned} I &= I_{ph} - I_d - I_P \\ &= I_{ph} - I_0 \left(e^{\frac{V_d}{nV_T}} - 1 \right) - \left(\frac{V + I \cdot R_S}{R_P} \right), \end{aligned} \quad (11)$$

where I_{ph} is related to both the total global irradiance on a tilted PV module (G_T) and the PV cell temperature (discussed in the previous two sections). I_d is defined by the Shockley diode equation, as in (11), which describes its voltage–current characteristic. I_0 is the reverse bias saturation current. V_T is the thermal voltage. Both I_0 and V_T are also proportional to the cell temperature. n is the diode ideality constant, which is between 1 and 2 [42].

To clarify the relation between the PV equivalent electric circuit model and the previous models of solar irradiance and PV cell temperature, more detailed sub-equations from (11) need to be described.

$$I_{ph} = \frac{G_T}{G_n} (I_{SC} + k_i (T_c - T_n)), \quad (12)$$

$$I_0 = \frac{I_{SC}}{e^{\frac{V_{OC}}{nV_T}} - 1} \cdot \left(\frac{T_n}{T_c} \right)^3 \cdot \exp \left(\frac{qE_g}{nk} \left(\frac{1}{T_n} - \frac{1}{T_c} \right) \right), \quad (13)$$

$$V_T = N_s \cdot \frac{kT_n}{q}, \quad (14)$$

where

- G_n : the irradiance under standard test conditions, STC;
- I_{SC} : the desired short-circuit current for the PV module;
- k_i : the temperature current constant in kelvin;
- T_n : the temperature under standard test conditions, STC, in kelvin;
- V_{OC} : the desired open-circuit voltage for the PV module;
- q : the electron's charge in coulomb (1.602×10^{-19} C);
- E_g : the band gap, 1.12 eV, for the silicon under standard test conditions, STC;
- k : the Boltzmann constant (1.38065×10^{-23} J/°K); and
- N_s : the number of series-connected cells in the PV module.

Now, the output electric power can be determined, as the MPP tracker is implemented to deliver the maximum possible power from the PV unit. The MPP curve is generated over the current–voltage characteristics of the PV cell, as shown in Figure 4. The power delivered by the module is the product of voltage (V) and current (I). The MPP is the rated power (P_R), which is caused by the product of the designated rated voltage (V_R) and rated current (I_R) under different circumstances. Several types of MPPT algorithms exist that can be applied, such as the perturbation and observation (P&O) technique, the incremental conductance technique, and fractional open-circuit voltage technique [43,44].

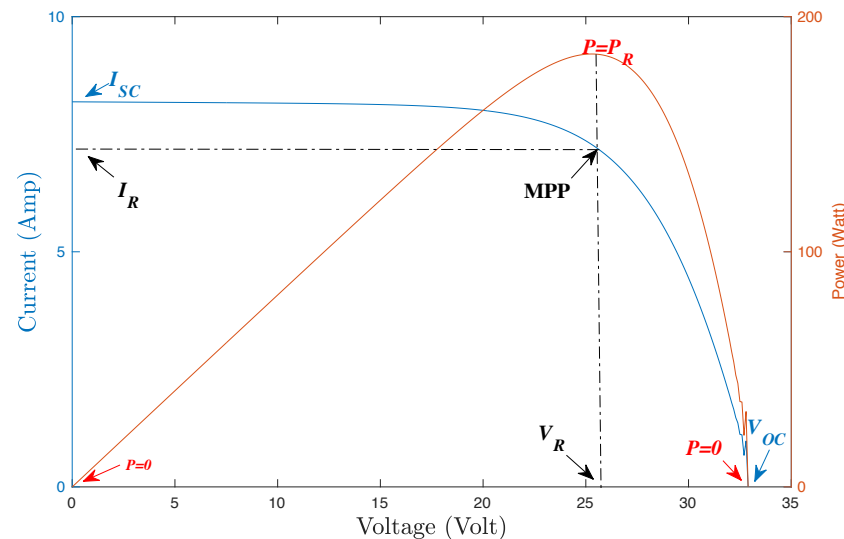


Figure 4. Current–voltage characteristic and power curves for a PV module.

3. PV Performance Investigation Analysis and Results

The analysis in this paper will be focused on the NEOM, the planned cross-border region in the Kingdom of Saudi Arabia, as a case study. The investigation of the optimal installation of solar modules in the NEOM is of great interest due to the announced ambitious plans for the energy system in the region. The goal is to build a 100% carbon-free powered region, with a great emphasis on leveraging both solar and wind energy sources. The region is planned to cover a total area of 26,500 km² and, thus, it is represented by three adjacent cities (i.e., Tabuk, Hagl, Duba) due to data availability constraints.

3.1. Solar Irradiance Absorbed by the Tilted PV Module

The PV irradiance model presented in Section II.A was implemented in MATLAB to simulate the impact of module tilt and azimuth angles on the amount of incident solar radiation on the PV module. Three-dimensional planes, shown in Figures 5–7, were plotted to demonstrate the sensitivity of the incident solar radiation to the variation in the tilt and azimuth angles for the locations studied: Tabuk, Hagl, and Duba. The incident solar radiation values were calculated for azimuth angles which ranged from -100° in the east direction to $+100^\circ$ in the west direction, relative to the direction due south, with 1-degree increments. Simultaneously, the analysis was carried out for the tilt angles, which ranged from 0° to 90° , with 1-degree increments.

Figure 5 shows the behavior of the incident solar radiation on the PV module with the variation in the tilt and azimuth angles at Tabuk. The PV module was exposed to a higher intensity of solar radiation when moving from the vertical to the inclined surface, where the solar intensity increased gradually as the tilt increased to approximately 30° . Then, it started to decrease. On the other hand, directing the PV module far away from due south, toward either the west or east, revealed that similar exposure of solar intensity was obtained. However, superior results were shown when the PV module was slightly directed to face southwest. Figures 6 and 7 show similar behaviors in Hagl and Duba, respectively.

Table 2 summarizes the results presented in Figures 5–7, which identified both the optimal tilt angle (β_{opt}) and optimal azimuth angle (γ_{opt}) in Tabuk, Hagl, and Duba, as well as their corresponding optimized achievable solar intensity. Indeed, with this, we have identified the optimal elevations and orientations that serve to maximize solar intensity on the PV module, which is crucial to maximizing the energy yield. In Tabuk, for instance, the annual optimal tilt angle, annual optimal azimuth angle, and solar intensity on the PV module were estimated to be 33° , 30° , and 3.6392 MWh/m^2 , respectively. The results in Hagl and Duba were relatively similar to those of Tabuk. The annual optimal tilt angle, annual optimal azimuth angle, and estimated solar intensity on the PV module in Hagl and Duba were determined to be 37° , 40° , and 3.4323 MWh/m^2 and 33° , 36° , and 3.4948 MWh/m^2 , respectively.

In addition, Table 2 shows that the simulated optimal tilt angle and azimuth were different from the location's latitude and were not in agreement with the rule-of-thumb direction for a PV module (i.e., facing due south). Furthermore, the significance between the amount of solar radiation falling on the PV panel at different setups (i.e., optimal tilt and azimuth angles setup and latitude tilt and south facing azimuth setup) was evaluated. It was found that the optimal tilt and azimuth angles contributed 0.91%, 4.01%, and 2.28% improvements in the amount of solar intensity on the PV panel in Tabuk, Hagl, and Duba, respectively.

Table 2. Optimal module tilt and azimuth angles to achieve maximum solar intensity.

Location	Tabuk (East of NEOM)	Hagl (North of NEOM)	Duba (South of NEOM)
Site latitude	28.38°	29.28°	27.34°
Optimal tilt angle (β_{opt})	33°	37°	33°
Optimal azimuth angle (γ_{opt})	30°	40°	36°
Optimized annual GHI (MWh/m^2)	3.6561	3.4586	3.5089
Annual GHI when elevation equal to latitude and facing due south (MWh/m^2)	3.6231	3.3254	3.4308
Achievable solar intensity improvement %	0.91	4.01	2.28

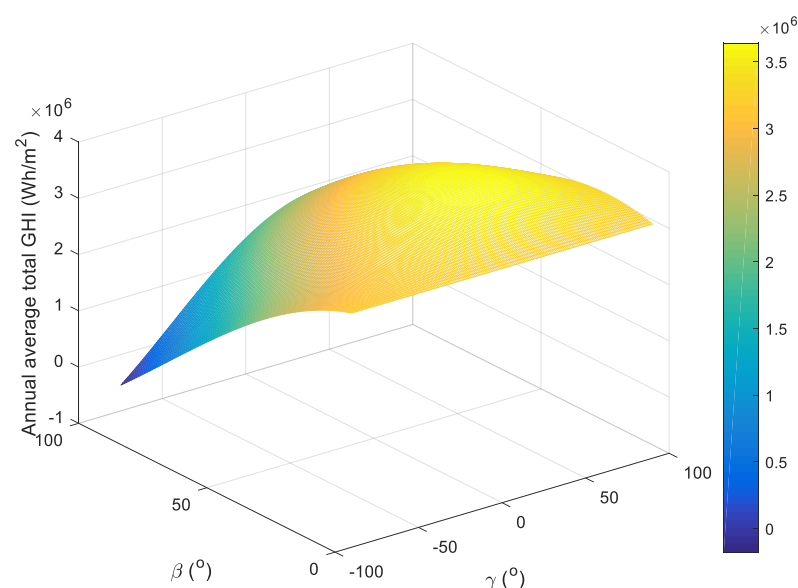


Figure 5. GHI in terms of tilt and azimuth angles in Tabuk.

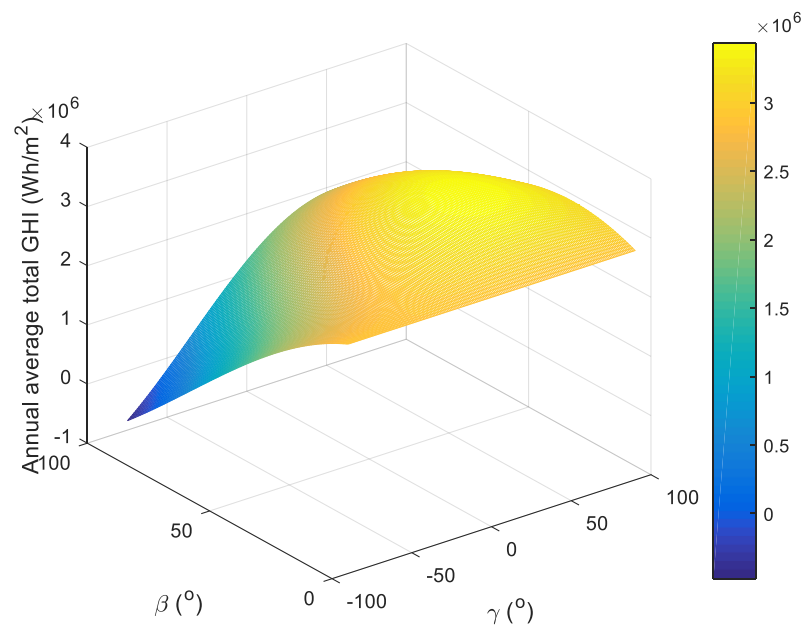


Figure 6. GHI in terms of tilt and azimuth angles in Hagl.

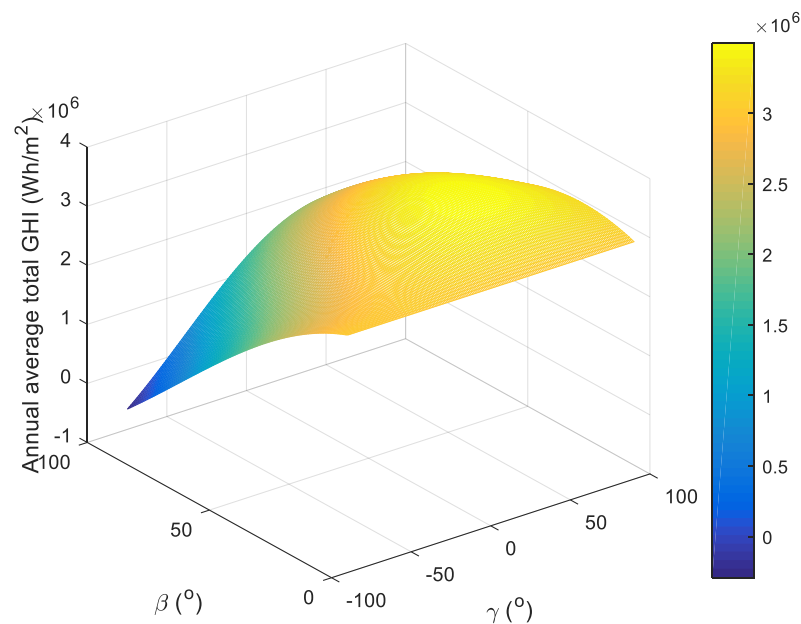


Figure 7. GHI in terms of tilt and azimuth angles in Dubai.

3.2. Impacts of Ambient Temperature and Local Wind Speed on PV Cell Temperature

The energy produced by a PV module is influenced by the variation between the PV cell temperature and the nominal operating cell temperature given by the manufacturer at standard test conditions (STC, as illustrated in Section 2.3). Therefore, the impact of the PV cell temperature must be parameterized in attempts to estimate the PV performance. The PV cell temperature is modeled as a function of solar radiation (G_T), ambient temperature (T_a), and wind speed (v_w), as discussed in Section 2.2.

Figure 8 illustrates the relationship between the PV cell temperature (T_c), ambient temperature (T_a), and wind speed (v_w) under the conditions listed in Section 2.2. More specifically, an increase in ambient temperature leads to a proportional elevation of the PV cell temperature, which impacts the PV module's performance. On the other hand, an increase in wind speed has a significant impact on the PV cell temperature, as a steep

decline in the PV cell temperature is observed in response to an increase in wind speed from 0 m/s to 10 m/s.

The significance of the PV cell temperature on the PV performance is given by Equation (10), which shows that it is crucial to take the PV cell temperature into consideration when attempting to estimate the PV module's performance.

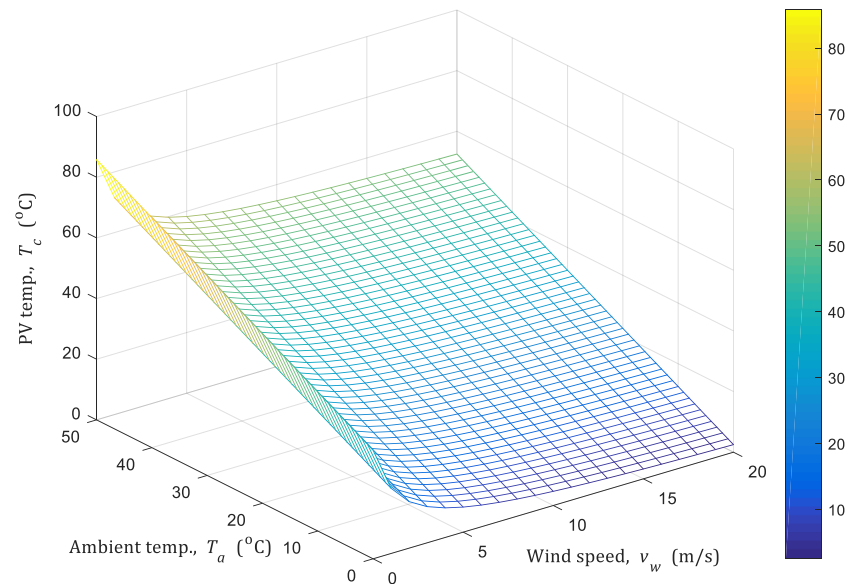


Figure 8. The impact of ambient temperature and wind speed on PV cell temperature.

3.3. PV Electric DC Power and Energy

In this section, we carry out power and energy performance analyses for the proposed equivalent DC circuit model of the PV cell, discussed in Section 2.3. More specifically, first, we obtained the monthly average energy density (Wh/m^2) for the PV output coupled with the GHI and GHI_t . Second, we evaluated the hourly power density (W/m^2) for the same three schemes.

To achieve more precise results, the specifications of a real 200 W manufactured PV module by SunPower (SPR-200-BLK-U) were applied throughout this model. Table 3 shows the values of the electrical parameters for this product.

Table 3. Electrical parameters for the SPR-200-BLK-U, manufactured by SunPower.

Parameter	Value
G_n	$1000 \text{ W}/\text{m}^2$
I_{SC}	5.4 A
k_i	$0.046 \text{ A}/^{\circ}\text{K}$
T_n	$298 \text{ }^{\circ}\text{K}$
V_{OC}	47.8 V
N_s	72 cells

Using the optimal tilt and azimuth angles, Figures 9–11 show the average monthly energy of the PV output, calculated directly from the maximum power point using the MPPT algorithm, which was then averaged over a month period to obtain the required energy density. For the input–output comparison, we also obtained the average monthly energy of the global irradiance for both the horizontal and tilted surfaces. As can be seen from the same figures (i.e., Figures 9–11), the average PV output energy achieved was around $110 \text{ Wh}/\text{m}^2$ throughout the year, since the studied locations were more or less

sunny all the year. However, we noticed that, in December, January, and February, the output energy was slightly higher than in the remaining months. Moreover, it is evident that the optimized tilt and azimuth angles yield higher *GHI*, which shows the importance of placing the panel at the proposed optimal angles.

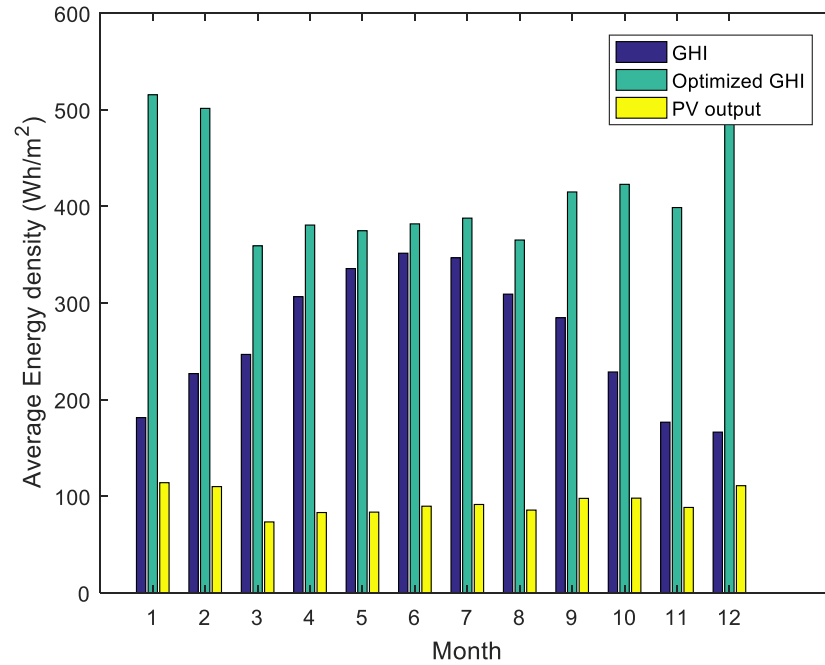


Figure 9. Average monthly energy density of the PV output for Tabuk.

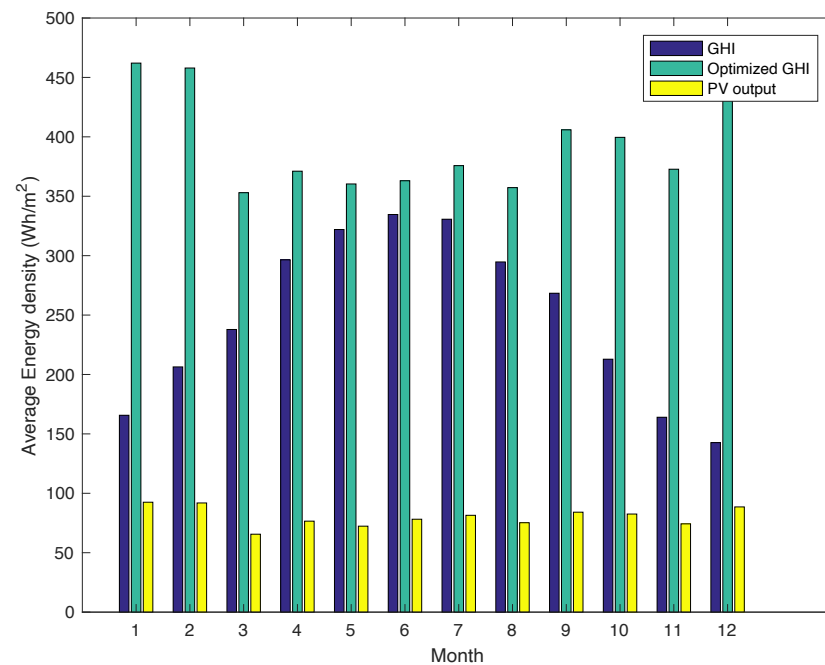


Figure 10. Average monthly energy density of the PV output for Hagl.

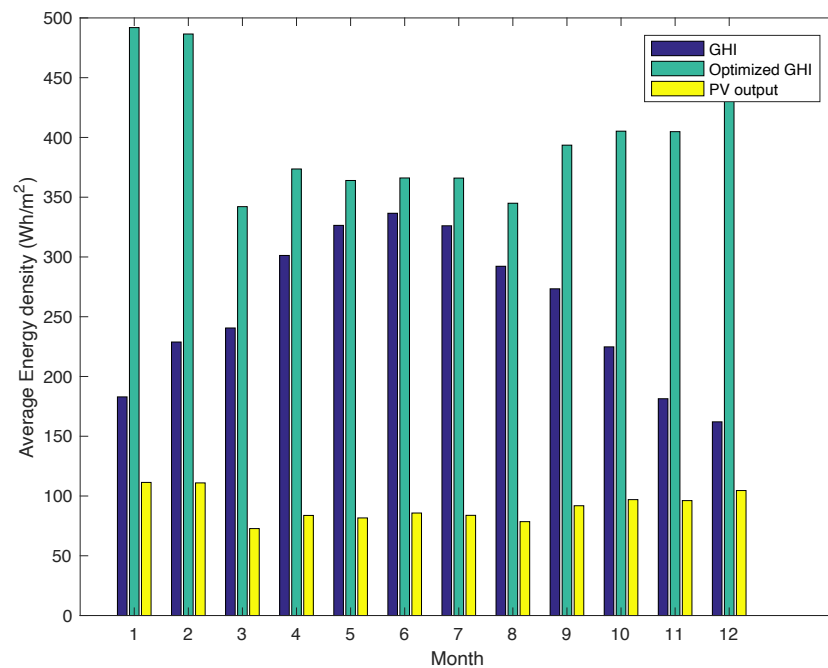


Figure 11. Average monthly energy density of the PV output for Dubai.

Similarly, the hourly power density of the PV module is depicted for a sample day in Figures 12–14. These figures show that the power values approximate the well-known bell-shape curve. In addition, the highest power that could be achieved with the chosen module was around 200 W/m^2 , at around 2:30 p.m. This observation was also applicable for both *GHI* and the optimized *GHI*, where the sun was in the middle of the sky.

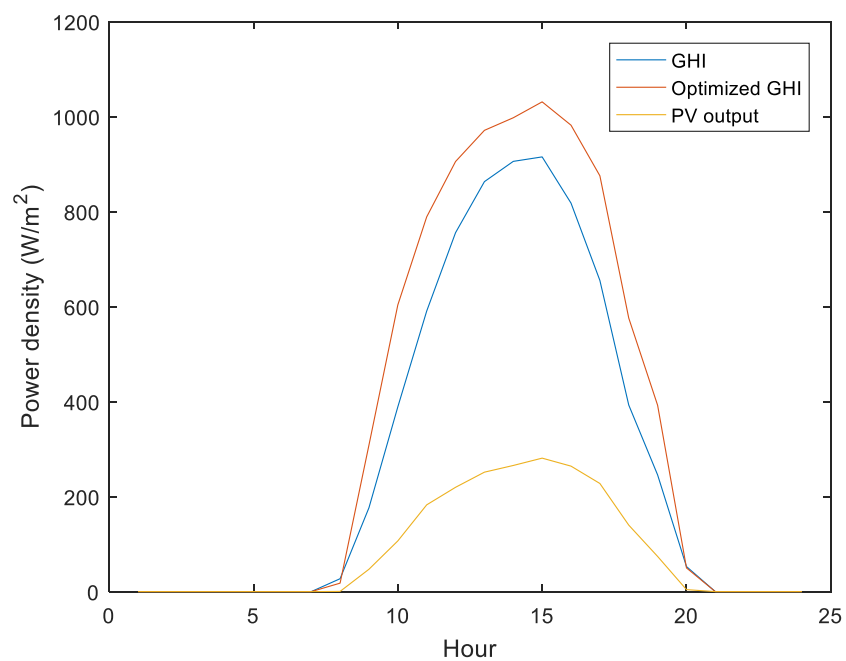


Figure 12. Hourly power density for a sample day in Tabuk.

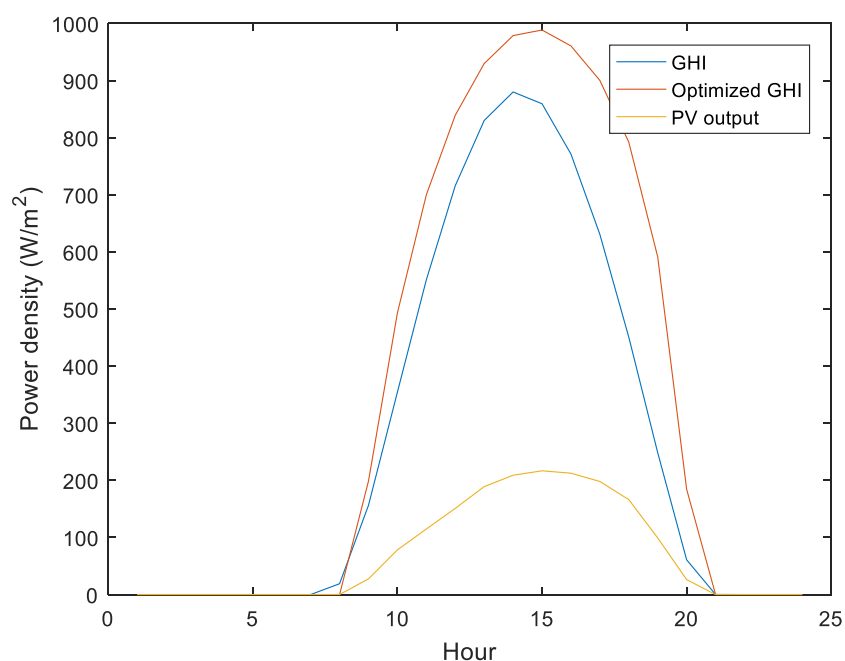


Figure 13. Hourly power density for a sample day in Hagl.

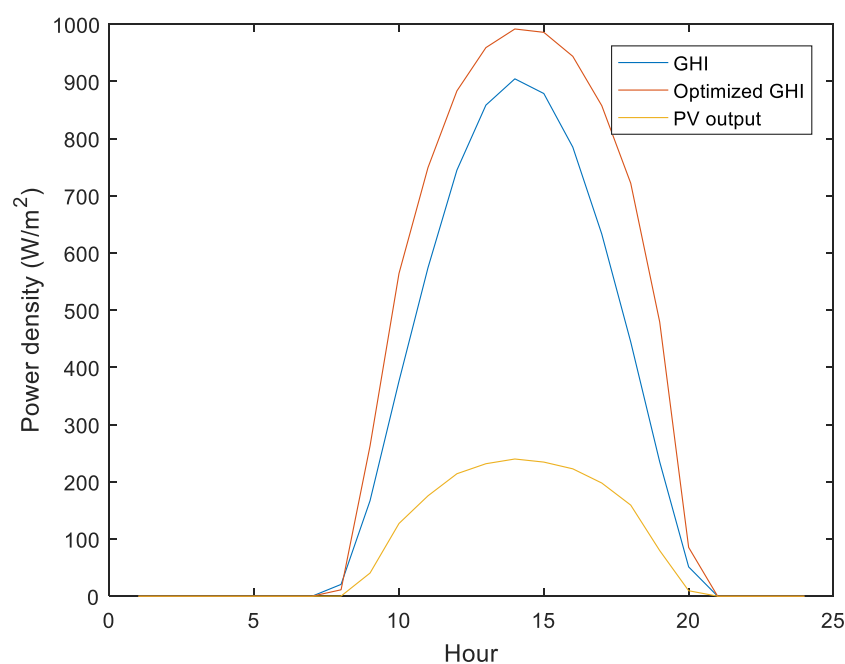


Figure 14. Hourly power density for a sample day in Duba.

From the discussions above, it was concluded that the proposed schemes discussed in Section 2, as well as the proposed optimal tilt and azimuth angles, can improve solar panel implementations in the chosen regions (i.e., Tabuk, Hagl, Duba).

4. Conclusions

In this paper, using real-time data, we studied how to improve the PV performance parameters in the NEOM region, namely: Tabuk, Hagl, and Duba. An optimization model, developed in MATLAB, is proposed to investigate the optimum values of the tilt angles combined with the azimuth angles. First, we proposed accurate mathematical models that precisely described the total global irradiance delivered to a tilted PV module. Second, we investigated the impact of the temperature of the PV cells on their performance and

provided a model that depicted the relationship between the PV cell temperature, ambient temperature, and wind speed. After determining the total irradiance delivered to the PV module and the PV cell temperature, we, third, developed an equivalent electric circuit for the PV cell and a maximum power point tracking algorithm. Fourth, we used these models to obtain the optimal tilt and azimuth angles that maximized the PV output of annual energy: 33° for both Tabuk and Duba and 37° for Hagl. Similarly, we found that the optimal azimuth angles were 30°, 40°, and 36° for Tabuk, Hagl, and Duba, respectively. Compared to elevation equal to the latitude and facing due south, it was shown that using the proposed optimal angles led to a 0.91%, 4.01%, and 2.28% improvement in the amount of solar intensity on the PV panel in Tabuk, Hagl and Duba, respectively. This, in turn, showed that the proposed schemes could be used to help design and implement solar panels in the studied region or any other location.

Author Contributions: Conceptualization, M.A., R.A. and A.A.; Methodology, M.A., R.A. and A.A.; Software, M.A. and A.A.; Formal analysis, M.A.; Resources, M.A.; Data curation, M.A., R.A. and A.A.; Writing—original draft, M.A., R.A. and A.A.; Writing—review & editing, M.A., R.A. and A.A.; Visualization, A.A.; Project administration, M.A. All authors have read and agreed to the published version of the manuscript.

Funding: This research received no external funding.

Institutional Review Board Statement: Not applicable.

Informed Consent Statement: Not applicable.

Data Availability Statement: Not applicable.

Acknowledgments: The authors would like to express their deepest appreciation to the King Abdullah City for Atomic and Renewable Energy K.A.CARE for providing access to the hourly solar irradiance data for Saudi Arabia. This research would not have been possible without this support.

Conflicts of Interest: The authors declare no conflict of interest.

References

1. Geels, F.W. Disruption and low-carbon system transformation: Progress and new challenges in socio-technical transitions research and the Multi-Level Perspective. *Energy Res. Soc. Sci.* **2018**, *37*, 224–231. [[CrossRef](#)]
2. Coady, D.; Parry, I.; Le, N.P.; Shang, B. *Global Fossil Fuel Subsidies Remain Large: An Update Based on Country-Level Estimates*; IMF Working Papers; IMF Working Paper Fiscal Affairs Department: Washington, DC, USA, 2019; Volume 19.
3. Kunreuther, H.; Gupta, S.; Bosetti, V.; Cooke, R.; Dutt, V.; Ha-Duong, M.; Held, H.; Llanes-Regueiro, J.; Patt, A.; Shittu, E.; et al. Integrated Risk and Uncertainty Assessment of Climate Change Response Policies. In *Climate Change 2014: Mitigation of Climate Change. Contribution of Working Group III to the Fifth Assessment Report of the Intergovernmental Panel on Climate Change*; Cambridge University Press: Cambridge, UK, 2014.
4. IEA. *World Energy Outlook 2019*; IEA: Paris, France, 2019.
5. IEA. *World Energy Outlook 2022*; IEA: Paris, France, 2022.
6. REN21. *Renewables 2022 Global Status Report*. 2022. Available online: <https://www.unep.org/resources/report/renewables-2022-global-status-report> (accessed on 15 June 2022).
7. Johansson, T.B.; Patwardhan, A.P.; Nakićenović, N.; Gomez-Echeverri, L. *Global Energy Assessment: Toward a Sustainable Future*; Cambridge University Press: Cambridge, UK, 2012.
8. IEA. *Chapter 2: Energy Sector Investment to Meet Climate Goals*; IEA: Paris, France, 2017.
9. Moriarty, P.; Honnery, D. Can renewable energy power the future? *Energy Policy* **2016**, *93*, 3–7. [[CrossRef](#)]
10. Capellán-Pérez, I.; de Castro, C.; Arto, I. Assessing vulnerabilities and limits in the transition to renewable energies: Land requirements under 100% solar energy scenarios. *Renew. Sustain. Energy Rev.* **2017**, *77*, 760–782. [[CrossRef](#)]
11. Dupont, E.; Koppelaar, R.; Jeanmart, H. Global available solar energy under physical and energy return on investment constraints. *Appl. Energy* **2020**, *257*, 113968. [[CrossRef](#)]
12. Kabir, E.; Kumar, P.; Kumar, S.; Adelodun, A.A.; Kim, K.H. Solar energy: Potential and future prospects. *Renew. Sustain. Energy Rev.* **2018**, *82*, 894–900. [[CrossRef](#)]
13. Fischer, M. ITRPV 11th edition April 2020 report presentation and key findings. In *Proceedings of the ITRPV Web-Seminar*, online, 9 June 2020.
14. Wang, X.; Barnett, A. The evolving value of photovoltaic module efficiency. *Appl. Sci.* **2019**, *9*, 1227. [[CrossRef](#)]
15. Benganem, M. Optimization of tilt angle for solar panel: Case study for Madinah, Saudi Arabia. *Appl. Energy* **2011**, *88*, 1427–1433. [[CrossRef](#)]

16. Heywood, H. Operating experiences with solar water heating. *IHVE J.* **1971**, *39*.
17. Chinnery, D.N.W. *Solar Water Heating in South Africa*; Council for Scientific and Industrial Research: Pretoria, South Africa, 1967; p. 79.
18. Lorsch, H. The use of solar energy for residential space heating. *Energy Convers.* **1973**, *13*, 1–5. [[CrossRef](#)]
19. Kern, J.; Harris, I. On the optimum tilt of a solar collector. *Sol. Energy* **1975**, *17*, 97–102. [[CrossRef](#)]
20. Nijegorodov, N.; Devan, K.R.; Jain, P.K.; Carlsson, S. Atmospheric transmittance models and an analytical method to predict the optimum slope of an absorber plate, variously oriented at any latitude. *Renew. Energy* **1994**, *4*, 529–543. [[CrossRef](#)]
21. Lewis, G. Optimum tilt of a solar collector. *Sol. Wind Technol.* **1987**, *4*, 407–410. [[CrossRef](#)]
22. El-Kassaby, M.M. Monthly and daily optimum tilt angle for south facing solar collectors; theoretical model, experimental and empirical correlations. *Sol. Wind Technol.* **1988**, *5*, 589–596. [[CrossRef](#)]
23. El-Kassaby, M.M.; Hassab, M.H. Investigation of a variable tilt angle Australian type solar collector. *Renew. Energy* **1994**, *4*, 327–332. [[CrossRef](#)]
24. Chiou, J.P.; El-Naggar, M.M. Optimum slope for solar insolation on a flat surface tilted toward the equator in heating season. *Sol. Energy* **1986**, *36*, 471–478. [[CrossRef](#)]
25. Elsayed, M.M. Optimum orientation of absorber plates. *Sol. Energy* **1989**, *42*, 89–102. [[CrossRef](#)]
26. Lv, Y.; Si, P.; Rong, X.; Yan, J.; Feng, Y.; Zhu, X. Determination of optimum tilt angle and orientation for solar collectors based on effective solar heat collection. *Appl. Energy* **2018**, *219*, 11–19. [[CrossRef](#)]
27. Elminir, H.K.; Ghitas, A.E.; El-Hussainy, F.; Hamid, R.; Beheary, M.M.; Abdel-Moneim, K.M. Optimum solar flat-plate collector slope: Case study for Helwan, Egypt. *Energy Convers. Manag.* **2006**, *47*, 624–637. [[CrossRef](#)]
28. Kaddoura, T.O.; Ramli, M.A.; Al-Turki, Y.A. On the estimation of the optimum tilt angle of PV panel in Saudi Arabia. *Renew. Sustain. Energy Rev.* **2016**, *65*, 626–634. [[CrossRef](#)]
29. Rowlands, I.H.; Kemery, B.P.; Beausoleil-Morrison, I. Optimal solar-PV tilt angle and azimuth: An Ontario (Canada) case-study. *Energy Policy* **2011**, *39*, 1397–1409. [[CrossRef](#)]
30. Tiwari, G.N.; Ahmad, M.J. Optimization of Tilt Angle for Solar Collector to Receive Maximum Radiation. *Open Renew. Energy J.* **2009**, *2*, 19–24. [[CrossRef](#)]
31. Elhassan, Z.A.M.; Zain, M.; Sopian, K.; Awadalla, A. Output energy of photovoltaic module directed at optimum slope angle in Kuala Lumpur, Malaysia. *Res. J. Appl. Sci.* **2011**, *6*, 104–109. [[CrossRef](#)]
32. Siddiqui, M.U.; Ali, S.; Khan, S.; Ali, S.; Horoub, M.M. Optimum Tilt Angles of Solar Collectors in Saudi Arabia. In Proceedings of the 2021 International Conference on Electrical, Communication, and Computer Engineering (ICECCE), Kuala Lumpur, Malaysia, 12–13 June 2021; IEEE: Piscataway, NJ, USA, 2021; pp. 1–5.
33. Garni, H.Z.A.; Awasthi, A.; Wright, D. Optimal orientation angles for maximizing energy yield for solar PV in Saudi Arabia. *Renew. Energy* **2019**, *133*, 538–550. [[CrossRef](#)]
34. Dey, S.; Lakshmanan, M.K.; Pesala, B. Optimal solar tree design for increased flexibility in seasonal energy extraction. *Renew. Energy* **2018**, *125*, 1038–1048. [[CrossRef](#)]
35. Ghosh, H.R.; Bhowmik, N.C.; Hussain, M. Determining seasonal optimum tilt angles, solar radiations on variously oriented, single and double axis tracking surfaces at Dhaka. *Renew. Energy* **2010**, *35*, 1292–1297. [[CrossRef](#)]
36. Cheng, C.L.; Jimenez, C.S.S.; Lee, M.C. Research of BIPV optimal tilted angle, use of latitude concept for south orientated plans. *Renew. Energy* **2009**, *34*, 1644–1650. [[CrossRef](#)]
37. Duffie, J.A.; Beckman, W.A. *Solar Engineering of Thermal Processes*, 4th ed.; John Wiley & Sons: Hoboken, NJ, USA, 2013. [[CrossRef](#)]
38. Hay, J.E.; Davies, J.A. Calculations of the solar radiation incident on an inclined surface. In Proceedings of the First Canadian Solar Radiation Data Workshop, Ottawa, ON, Canada, 17–19 April 1980.
39. Loferski, J.; Ahmad, J.; Pandey, A. Performance of photovoltaic cells incorporated into unique hybrid photovoltaic/thermal panels of a 2.8 kW residential solar energy conversion system. In *Proceedings of the 1988 Annual Meeting*; American Solar Energy Society: Cambridge, MA, USA, 1988; pp. 427–432.
40. Ridha, H.M.; Hizam, H.; Mirjalili, S.; Othman, M.L.; Ya'acob, M.E.; Abualigah, L. A Novel Theoretical and Practical Methodology for Extracting the Parameters of the Single and Double Diode Photovoltaic Models. *IEEE Access* **2022**, *10*, 11110–11137. [[CrossRef](#)]
41. Gilbert, M.M. Renewable and efficient electric power systems. *Choice Rev. Online* **2005**, *42*. [[CrossRef](#)]
42. Shockley, W. The Theory of p-n Junctions in Semiconductors and p-n Junction Transistors. *Bell Syst. Tech. J.* **1949**, *28*, 435–489. . [[CrossRef](#)]
43. ESRAM, T.; Chapman, P.L. Comparison of photovoltaic array maximum power point tracking techniques. *IEEE Trans. Energy Convers.* **2007**, *22*, 439–449. [[CrossRef](#)]
44. Hussein, A.A.; Chen, X.; Alharbi, M.; Pise, A.A.; Batarseh, I. Design of a Grid-Tie Photovoltaic System with a Controlled Total Harmonic Distortion and Tri Maximum Power Point Tracking. *IEEE Trans. Power Electron.* **2020**, *35*, 4780–4790. [[CrossRef](#)]

Disclaimer/Publisher's Note: The statements, opinions and data contained in all publications are solely those of the individual author(s) and contributor(s) and not of MDPI and/or the editor(s). MDPI and/or the editor(s) disclaim responsibility for any injury to people or property resulting from any ideas, methods, instructions or products referred to in the content.